Transition between large and small electron polaron at neutral ferroelectric domain walls in $BiFeO_3$

Sabine Körbel
School of Physics, AMBER and CRANN Institute, Trinity College, Dublin 2, Ireland and
Institute of Physics, Academy of Sciences of the Czech Republic, Na Slovance 2, 182 21 Prague 8, Czech Republic

Jirka Hlinka
Institute of Physics, Academy of Sciences of the Czech Republic, Na Slovance 2, 182 21 Prague 8, Czech Republic

Stefano Sanvito
School of Physics, AMBER and CRANN Institute, Trinity College, Dublin 2, Ireland

Ferroelectric domain walls are planes within an insulating material that can accumulate and conduct charge carriers, hence the interaction of the domain walls with the charge carriers can be important for photovoltaic and other electronic applications. By means of first principles calculations we predict a transition from a large two-dimensional electron polaron to a small polaron at the domain walls at a critical electron density, with polaron signatures in optical absorption and photoluminescence. We find that large and small polarons at the domain walls create different absorption peaks within the band gap that are not present in the case of pristine domain walls. These are an extended Drude peak in the case of large electron or hole polarons and a narrow mid-gap peak in the case of the small electron polaron.

I. INTRODUCTION

Novel photovoltaic absorber materials and materials engineering concepts may help to make photovoltaics more efficient and more versatile. Ferroelectric photovoltaics might be one of such future photovoltaic technologies. Ferroelectric photovoltaics are promising because they could provide three solar-cell functions within one material, namely the generation, separation, and conduction of photocharge carriers. The ferroelectric material provides the bulk photovoltaic effect [1–3], and the ferroelectric domain walls may, in principle, both separate and conduct the photogenerated charge carriers [2, 4, 5]. The domain walls may hence be the most active areas within the ferroelectric, where most of the charge carrier dynamics take place. Recently we discovered a transition between large and small exciton polarons at neutral ferroelectric domain walls in $BiFeO_3$ [5]. A similar transition occurs for electron polarons, as we will show here.

Charge carriers in nanostructured semiconductors or insulators can be monitored for example by means of spatially resolved optical absorption or photoluminescence spectroscopy. For ferroelectric domain walls this is challenging because the domain walls are atomically narrow, and because optical signatures of charge carriers at domain walls may be difficult to distinguish from those at point defects. Here we use first principles modelling based on density-functional theory (DFT) to identify optical signatures of charge carriers at pristine ferroelectric domain walls in $BiFeO_3$, one of the most studied ferroelectric photovoltaic materials.

$BiFeO_3$ is a prototype ferroelectric photovoltaic with a very stable and large ferroelectric polarization close to 100 μC/cm^2 [6], a high ferroelectric Curie temperature above 1100 K [7], and a relatively small direct optical band gap, compared to most other ferroelectric oxides, of ≈2.7–3.0 eV [8–14]. $BiFeO_3$ can therefore be considered a starting point for tailoring ferroelectric photovoltaic absorber materials, even though its bandgap is still too large for an efficient harvesting of visible light.

$BiFeO_3$ exhibits a bulk photovoltaic effect due to its non-centrosymmetric *R*3*c* crystal structure [1–3, 15]. Additionally, a contribution from ferroelectric domain walls to the photovoltage has been proposed [16–18]. The atomic structures and formation energies of low-energy ferroelectric domain walls in $BiFeO_3$ are well known [4, 19–22]. Three types of domain walls can form with different angles between the polarization directions in adjacent domains: 71°, 109°, and 180°, all of which are experimentally observed [4, 21, 23]. It was previously found that holes in $BiFeO_3$ form large polarons only [24, 25]. Domain walls are two-dimensional electron (and hole) traps [24], which makes it possible to study electron polarons at high local electron densities. Here we investigate the small electron polaron at the domain wall and find that it forms only above a critical electron density, and we predict if and how electron and hole polaron states in $BiFeO_3$ can be detected in optical absorption and photoluminescence spectra. Throughout this work we will distinguish "small" and "large" polarons by the spatial extension of the electronic wave function compared to the interatomic distances (small polaron: localized within maximally a few interatomic distances; large polaron: delocalized over ≥ tens of interatomic distances).

II. METHODS

A. Ground state properties

We consider charge-neutral and "mechanically compatible" [19, 26] ferroelectric domain walls in lattice planes with low Miller indices as the most abundant types of domain walls. All calculations were performed with the program VASP [27], using the Projector-Augmented Wave (PAW) method and pseudopotentials with 5 (Bi), 16 (Fe), and 6 (O) valence electrons, respectively. We used the local spin-density approximation (LSDA) to density-functional theory (DFT), and corrected

the band gap with a Hubbard-U of 5.3 eV using Dudarev's scheme [28]. This U value was taken from the materials project [29] and it is optimized for oxide formation energies, but also yields band gaps and ferroelectric polarization close to experiment. With our U we obtain a ferroelectric polarization of $\approx 94\,\mu$C/cm^2 [5] (Expt.: $\approx 100\,\mu$C/cm^2 [6]). Spin-orbit coupling was neglected. The reciprocal space was sampled with a k-point grid equivalent to about $7\times7\times7$ k-points for a 5-atom perovskite unit cell. Plane-wave basis functions with energies up to 520 eV were used. We employed supercells of 120 atoms with periodic boundary conditions, such that every supercell contained two domain walls. Both the atomic positions and the cell parameters were optimized until the total energy differences between consecutive iteration steps fell below 0.01 meV for the optimization of the electronic density and below 0.1 meV for the optimization of the atomic structure. The antiferromagnetic G-type spin configuration of the bulk was maintained in the systems with domain walls. Atomic and electronic structure of the domain-wall systems investigated here have been published elsewhere [19, 21, 24]. The valence band maximum (VBM) and the conduction band minimum (CBM) of $BiFeO_3$ are largely comprised of p-type states located on oxygen and d-type states located on Fe, respectively. This is also the case for pristine domain walls. Here we considered systems without any excess charge carriers as well as those with excess electrons or holes, corresponding to n-doped or p-doped conditions, respectively. To this end, electrons were added or removed from the system, and a uniform compensating background charge density was added. The structures with excess charges were optimized in order to take into account polaron formation. Excess charges between 0.1 and 1 electron or hole in the supercell were considered.

B. Optical properties

Since our system size is large and our study is computationally expensive already at the DFT level, we do not employ many-body perturbation theory to calculate optical properties. Instead we use the independent-particle approximation to calculate the frequency-dependent imaginary part of the dielectric permittivity, $\varepsilon_2(\omega)$, thereby neglecting excitonic effects, and we also neglect local-field effects, which should be small in the case of materials with small optical anisotropy, such as $BiFeO_3$. In this case ε_2 is given by

$$\varepsilon_2^{\alpha\beta}(\omega) = \frac{4\pi^2e^2}{\Omega}\lim_{\mathbf{q}\to\mathbf{0}}\frac{1}{q^2}\sum_{c,v,\mathbf{k}} 2w_{\mathbf{k}}\delta(\epsilon_{c\mathbf{k}}-\epsilon_{v\mathbf{k}}-\omega) \cdot\langle u_{c\mathbf{k}+\mathbf{e}_\alpha q}|u_{v\mathbf{k}}\rangle\langle u_{c\mathbf{k}+\mathbf{e}_\beta q}|u_{v\mathbf{k}}\rangle^*, \quad (1)$$

where α and β are cartesian directions, v and c are valence- and conduction-band indices at k-point $\mathbf{k}$, the $\epsilon_{n\mathbf{k}}$ are energy eigenvalues, u is the lattice-periodic part of the Bloch function, $\mathbf{e}$ is a cartesian unit vector, Ω is the unit-cell volume, and $w_{\mathbf{k}}$ is the k-point weight. The real part of the dielectric permittivity ε_1, needed to calculate the absorption coefficient, was obtained from a Kramers-Kronig transformation [30]. Unless specified otherwise, broadening of the order of 0.1 eV was applied to the optical spectra in order to mimick broadening effects present in experimental spectra. The absorption coefficient α is given by

$$\alpha = \frac{4\pi\nu\kappa}{c}, \quad (2)$$

where ν is the frequency of the incident light, c is the speed of light, and $\kappa = \sqrt{(|\varepsilon|-\varepsilon_1)/2}$ is the imaginary part of the complex index of refraction [31]. In order to obtain a direction-averaged dielectric permittivity and absorption coefficient, we average the eigenvalues of the dielectric matrix, ε_2.

In order to qualitatively estimate how the weight of the polaron peak might be enhanced in photoluminescence with respect to optical absorption spectra, we weighted the absorption spectra by a Bose-Einstein distribution function of the exciton energies as it was proposed in Ref. 32. It should be noted that this approach may not be sophisticated enough to yield correct orders of magnitude.

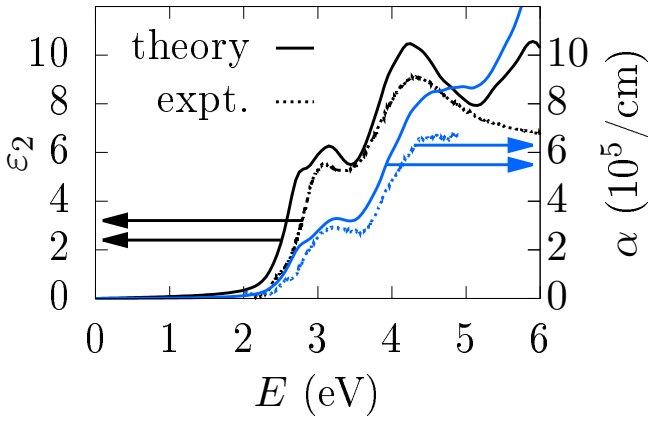

FIG. 1. (Color online) Imaginary part of the dielectric permittivity ε_2 (left axis) and absorption coefficient α (right axis) from theory (solid lines) and experiment (dotted lines). Experimental spectra are taken from Ref. 10 (ε_2) and Ref. 8 (α).

III. RESULTS AND DISCUSSION

A. Optical spectra of the bulk

First we validate our computational parameters by comparing the calculated optical spectrum of the bulk crystal with the experimentally measured one. Figure 1 shows the imaginary part of the dielectric permittivity (left axis) and the absorption coefficient (right axis). The calculated spectrum is the average over cartesian directions. The main absorption onset (direct band gap) of thin films of $BiFeO_3$ was found at about 2.7–2.8 eV [8–11, 13]. The calculated spectrum agrees reasonably well with the experimentally measured one, even though it is redshifted by about 0.2 eV. From a Tauc plot we obtain a direct optical band gap of 2.54 eV. This is higher than our calculated direct band gap of 2.25 eV (our calculated fundamental band

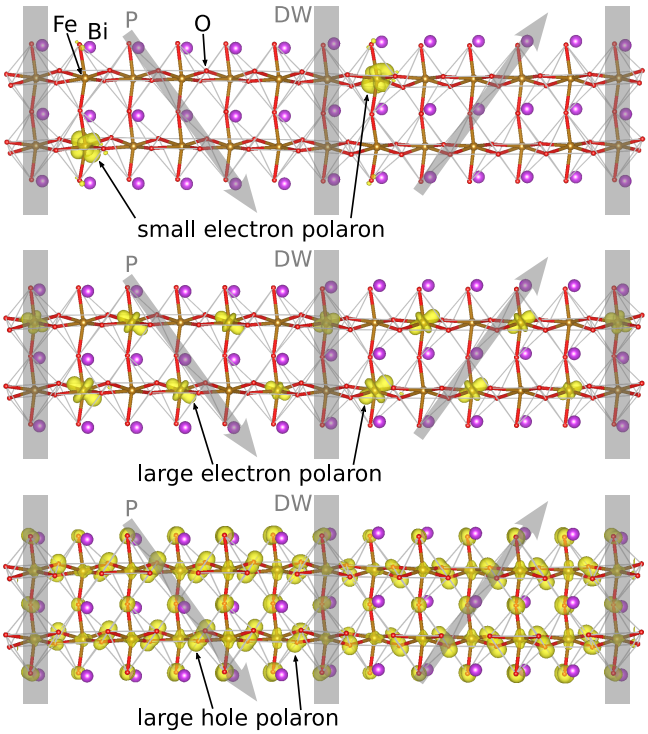

FIG. 2. (Color online) 71° domain wall with small electron polarons (top), large electron polarons (center), and large hole polarons (bottom). The yellow objects are charge density iso-surfaces of the excess electron or hole, respectively. Gray bars and arrows indicate domain walls ("DW") and polarization ("P") directions, respectively.

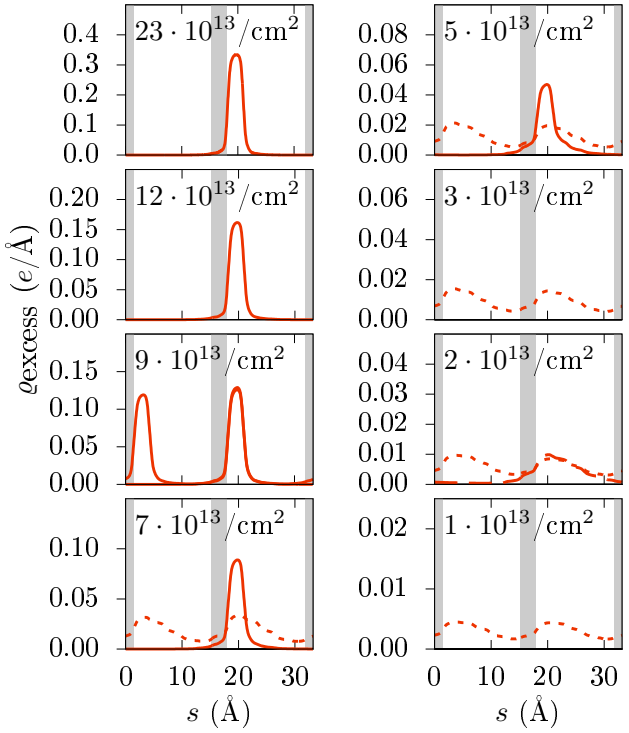

FIG. 3. (Color online) Line density (in-plane average) of the excess electrons for planar electron densities ranging from $\approx$ 1 to $23 \cdot 10^{13}$ electrons/cm^2. Gray bars mark 71° domain walls. Solid lines: small polarons, dashed lines: large polarons. The densities were smoothened by applying a sliding-window average with a window size of one atomic layer spacing.

gap is 2.18 eV), indicating that the lowest-energy direct transitions between the band edges are dipole-forbidden. It should be noted that a larger Hubbard U would increase the optical gap and hence move it closer to experiment, whereas including spin-orbit coupling would decrease the gap [33]. While a larger Hubbard U would yield an optical gap closer to experiment, our slightly smaller U, which yields simultaneously formation energies, band gaps, and ferroelectric polarization close to experiment, is more likely to yield robust results for other properties as well, such as polaron properties.

B. Polarons at domain walls

Having validated our computational parameters, we now consider domain-wall systems. We find that both large and small electron polarons can be stable depending on the concentration of excess electrons, whereas holes always form large polaron states, in agreement with findings in Ref. 25. The large electron and hole polarons occupy metal-like states at the bottom of the conduction band (electron) or the top of the valence band (hole), respectively, whereas the small electron polaron occupies a mid-gap state such that the system retains a finite band gap [24]. In Fig. 2 the atomic configuration of the 71° domain wall is shown. The figure also shows iso-surfaces of the charge densities of excess electrons and holes.

1. *Transition between large and small electron polarons*

Upon varying the planar electron density in the domain wall we find a transition between the large and the small electron polaron at a critical electron density. Figure 3 shows the line density (the in-plane average) of the excess electron. For intermediate electron densities of about 3 to $9{\cdot}10^{13}$ electrons/cm^2, depending on the starting configuration, both the large and the small electron polaron can be obtained, whereas for electron densities outside this range only one of the two polaron types is stable. For a density of $\geq 9 \cdot 10^{13}/\mathrm{cm}^2$ the initial configuration with a delocalized excess charge density spontaneously transforms into a small polaron state, whereas for $\leq 3{\cdot}10^{13}/\mathrm{cm}^2$ we can only obtain the large polaron. If starting from the atomic configuration of a small polaron with larger electron density, we obtain a large polaron at one of the domain walls, whereas when starting from the delocalized excess electron we obtain a large polaron state split over both domain walls.

Figure 4 shows the normalized energy difference between the large and the small electron polaron as a function of the planar electron density in the domain wall, $\Delta E = \left(E_{\mathrm{tot}}^{\mathrm{polaron}} - E_{\mathrm{tot}}^{\mathrm{ground\ state}}\right)/N_e - E_F^{\mathrm{ground\ state}}$. Here N_e is the number of electrons in the supercell. We take the Fermi energy E_F of the ground state as the energy reference in or-

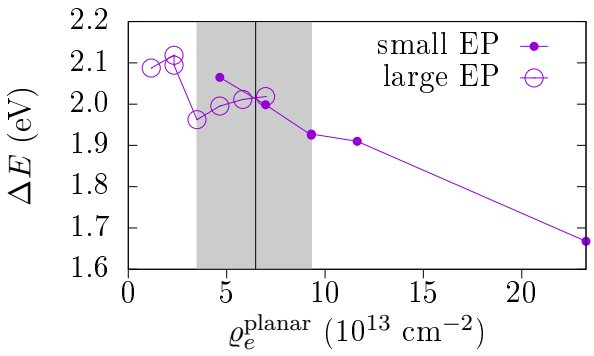

FIG. 4. (Color online) Energy difference ΔE between small and large electron polaron ("EP") at the 71° domain wall as a function of the planar electron density in the domain wall. The vertical black line marks the critical planar density, the gray shaded area marks the coexistence region.

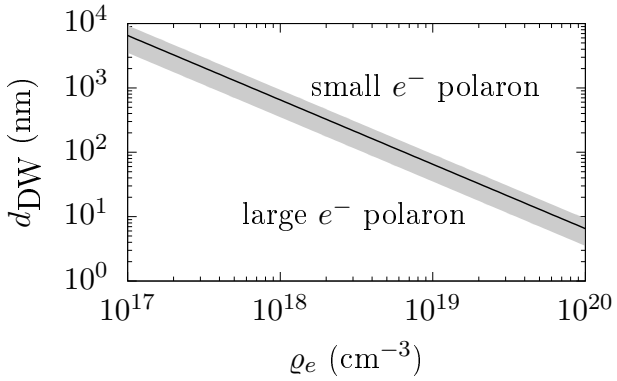

FIG. 5. (Color online) Phase diagram for the electron polaron at the 71° domain wall. The black line marks the domain-wall spacing at which the large-to-small polaron transition occurs, as a function of the electron doping level. The gray shaded area is the coexistence region of large and small polaron.

der to remove the arbitrary shift in the total energy that is present in our computational approach. In this way we can observe how ΔE approaches the band gap energy in the limit of low excess electron densities, as one would expect it to. The transition from the large to the small polaron takes place somewhere inside the coexistence region between about 3 and $9{\cdot}10^{13}$ electrons/cm^2. We estimate that it lies at about $7{\cdot}10^{13}$ electrons/cm^2, where the formation energies of SEP and LEP are equal. In principle the critical electron density could be affected by a spurious polaron-polaron interaction caused by a too small domain wall spacing in the simulation. However, this is not the case: For two densities, 2 and $9{\cdot}10^{13}$ electrons/cm^2, we considered both the case that every domain wall hosts a polaron and the case that only every other domain wall hosts a polaron. Both the shape of the electron density (Fig. 3) and the formation energies (Fig. 4) are almost identical for the original and the doubled polaron-polaron distance for these two densities.

Assuming that all excess electrons in the material are trapped in the domain walls, then the relation between doping level ϱ_e, planar electron density in the domain wall $\varrho_e^{\text{planar}}$, and domain wall spacing d_{DW} is simply $\varrho_e = \varrho_e^{\text{planar}}/d_{\text{DW}}$. This yields the critical doping level as a function of the domain-wall spacing, as depicted in Fig. 5. For a typical domain-wall spacing of the order of 100 nm the transition occurs at a doping level of the order of 10^{18} to 10^{19} cm^{-3}. Figure 6 shows the density of states (DOS) of the electron polaron for different planar electron densities. The large polaron leaves the DOS nearly unaffected, regardless of the electron density. This is different in the case of the small polaron, where at $\approx 5 \cdot 10^{13}$ electrons/cm^2 a peak forms at the bottom of the conduction band, which detaches from the conduction band minimum at $\approx 7 \cdot 10^{13}$ electrons/cm^2 electrons in the supercell and moves deeper down into the band gap with increasing electron density. At a density of $\approx 2 \cdot 10^{14}$ electrons/cm^2 the level of the small polaron lies deep within the band gap, and a second level has appeared above the valence band maximum.

2. *Polarons in optical spectra*

Figure 7 shows the optical spectra (imaginary part of ε) of $BiFeO_3$ without ("bulk") and with domain walls ("DW"), and the difference between them. The optical spectrum of the pristine domain wall is nearly identical to that of the bulk. This is different when excess electrons or holes are present. Both the large electron polaron and the large hole polaron state lead to large absorption at vanishing photon energy due to their metal-like nature (Drude peak). In the case of the small electron polaron there is no Drude peak, instead we find an absorption peak at a photon energy of $\approx$ 1.1 eV (71° and 180° domain wall) and 1.0 eV (109° domain wall), which is well separated in energy from the rest of the spectrum and which might therefore be detectable by optical absorption or photoluminescence spectroscopy. Given the limited accuracy of the level of theory adopted here, and the fact that the peak position depends on the electron density (see Fig. 6), the peak may in practice be slightly shifted with respect to our prediction, but it lies deep in the band gap, well separated from the conduction band minimum. For better visibility of the polaron peaks we also show the differential spectra ($\Delta\varepsilon_2 = \varepsilon_2 - \varepsilon_{2,\text{bulk}}$) in the bottom panels of Fig. 7. The small electron polaron peak is composed of electronic transitions between the small electron polaron level and the lowest conduction bands, as depicted in Fig. 8, which shows ε_2 around the small polaron peak, the electronic density of states (DOS), and the contribution $\tilde{\varepsilon_2}$ to ε_2 that stems only from electronic transitions between states within the red rectangle, that is, between the polaron level just below 0 eV and the lowest conduction bands near 1 eV. The spectra of the 109° and 180° domain walls are very similar to that of the 71° wall. The most pronounced effects of the domain walls are the additional absorption peaks stemming from small electron polarons and metal-like large hole and electron polaron states, respectively, which are very similar for all three walls. The small electron polaron state contributes only a tiny fraction of the total absorption spectrum: Even if a spatially resolved absorption spectrum was

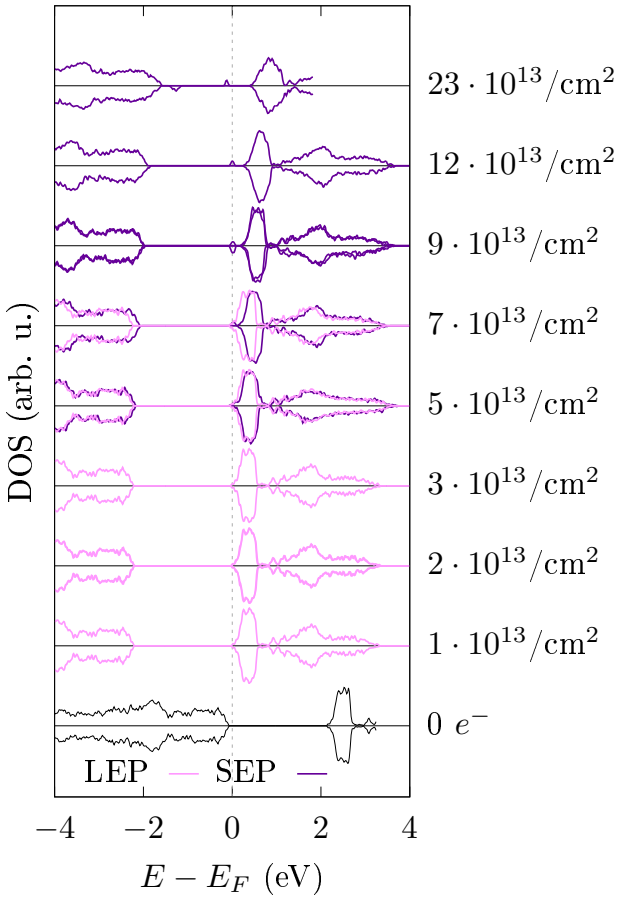

FIG. 6. (Color online) Density of states (DOS) of electron polarons at the 71° domain wall for different planar electron densities. Black solid line: without polaron, dark purple lines: small electron polaron (SEP); pink lines: large electron polaron (LEP). Spin-down DOS were multiplied by -1 for better visibility. The DOS were vertically shifted for better visibility.

taken in a spatial region spanning only several nanometers centered at the domain wall, the amplitude of the mall polaron peak would only be at a few percent of that of the main peaks. This idealized situation is the one shown in Fig. 7. In a macroscopic absorption spectrum, or one with a spatial resolution of hundreds of nanometers, the peak would be even much smaller, below 0.1% for a doping level of $10^{18}\,\mathrm{cm}^{-3}$ and a domain wall spacing of about 200 nm. Therefore this peak will be difficult to detect in absorption spectroscopy, but much easier using photoluminescence spectroscopy. Figure 9 shows qualitatively estimated photoluminescence ("QE-PL") spectra of the bulk and the domain walls with small electron polarons together with experimental data of Ref. 14 for the single-domain bulk. Other than in the absorption spectrum, in the estimated photoluminescence spectrum the peak of the small electron polaron near 1 eV is very pronounced. There is at a similar position a peak in the experimental spectrum that was assigned to oxygen vacancies, which might hide the polaron peak stemming from domain walls. In fact, the properties (energy level and shape of the wave function) of small electron polarons at oxygen vacancies [34] are very similar to those of small electron polarons at domain walls, indicating that the properties of the small electron polaron may be largely independent of the nature of the electron trap. There is however a difference between the small electron polaron at domain walls and at oxygen vacancies: the energy level of the small polaron at the domain wall depends continuously on the density of electrons at the domain wall (see Fig. 6), and in planar traps like domain walls the electron density, and hence the energy level of the polaron, can be tuned quasi-continuously. This is different from zero-dimensional traps like oxygen vacancies, for which only a few discrete electron densities are possible (zero, one, or two electrons per trap in this case), and the polaron levels can only attain a few discrete values. Experimentally the polaron peak at domain walls could perhaps be distinguished from that at oxygen vacancies by comparing spectra of electron-doped $BiFeO_3$ with domain walls (peaks from both polarons and oxygen vacancies) and without domain walls (peak only from oxygen vacancies) under oxygen-rich conditions that minimize the accumulation of oxygen vacancies at the domain walls.

IV. SUMMARY AND CONCLUSIONS

If ferroelectric domain walls are present in $BiFeO_3$, excess electrons or holes will accumulate there. Holes form only large polarons, both at the domain walls and in the bulk [25]. Electrons also form large polarons at the domain walls as long as the electron density in the wall is low enough. However, if the electron density in the domain wall exceeds a critical value (if the doping level is high, or if there are not too many domain walls), then the large electron polaron undergoes a transition to a small electron polaron. We find the critical planar electron density in the domain wall for this transition to occur to be about $7 \cdot 10^{13}\,\mathrm{cm}^{-2}$. This critical planar density could be reached, for example, for an electron doping level of the order of 10^{18} to $10^{19}\,\mathrm{cm}^{-3}$ and a domain wall spacing of ≈ 100 to 1000 nm, if the domain walls are the prevailing electron traps.

Optical absorption and photoluminescence spectra of $BiFeO_3$ could reveal the nature of excess charge carriers at the ferroelectric domain walls. In the case of hole doping (p-type conditions), a Drude peak appears due to the metal-like density of states of the large hole polaron. A similar Drude peak appears for the large electron polaron. If the electron density in the wall exceeds the critical density and the large polaron transforms into a small one, the Drude peak vanishes, and instead a single peak appears deep inside the band gap, which is the signature of the small electron polaron. Whereas this peak is small and may not be easy to detect in absorption spectra, the same peak should be much more pronounced, maybe even dominant in photoluminescence spectra, even at room temperature or above. A similar large-to-small polaron transition and metal-insulator transition were also predicted at charged domain walls in $PbTiO_3$ [35], indicating that these may be an ubiquitous phenomenon at planar electron traps in electron-doped perovskite oxides. Undoped neutral ferroelec-

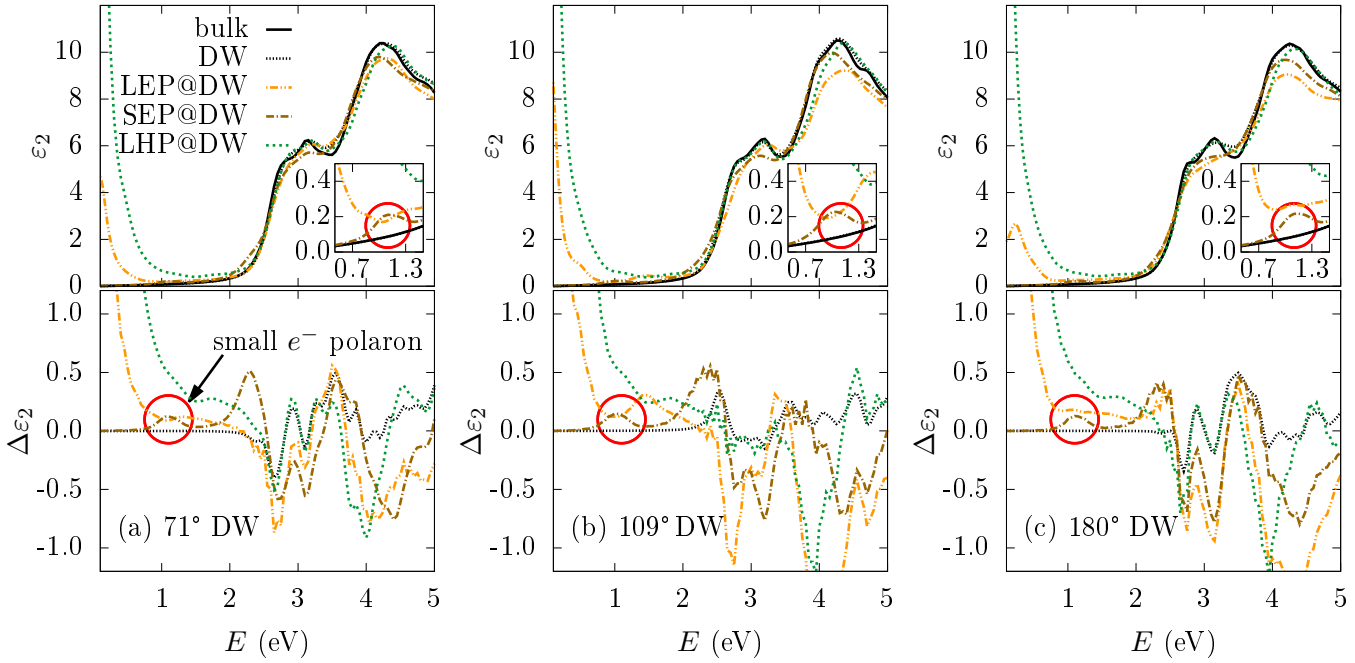

FIG. 7. (Color online) Imaginary part of the microscopically averaged dielectric permittivity, ε_2, of $BiFeO_3$ without ("bulk") and with domain walls ("DW") and with small ("SEP") and large ("LEP") electron polarons and large hole polarons ("LHP") at the domain walls. (a) 71° wall; (b) 109° wall; (c) 180° wall. The bottom panels show differential spectra with respect to those of the bulk ($\Delta\varepsilon_2 = \varepsilon_2 - \varepsilon_{2,\text{bulk}}$). Red circles mark peaks from small electron polarons. The dielectric permittivity is averaged over a narrow (≈ 2 nm wide) spatial region centered at the domain wall.

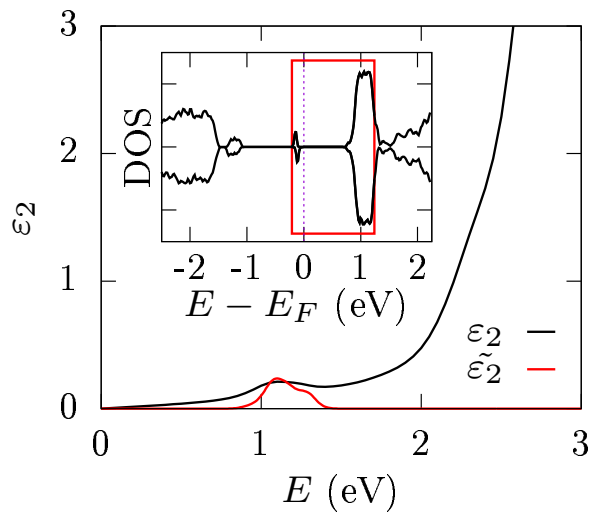

FIG. 8. (Color online) Imaginary part of the dielectric permittivity ε_2 for the small electron polaron at the 71° wall. The inset shows the electronic density of states (DOS) in arbitrary units. $\tilde{\varepsilon}_2$ is the part of ε_2 that stems only from electronic transitions between states within the red rectangle. E_F is the Fermi energy. A Gaussian broadening of 25 meV was applied to $\tilde{\varepsilon}_2$.

tric domain walls do not have any pronounced effect on the the optical spectrum of $BiFeO_3$.

ACKNOWLEDGEMENT

This project has received funding from the European Union's Horizon 2020 research and innovation programme under the Marie Skłodowska-Curie Grant Agreement No. 746964 and from the Czech Science Foundation (Project No. 15-04121S). Computational resources and support were supplied by the Trinity Centre for High Performance Computing funded by Science Foundation Ireland, the Irish Centre for High-End Computing, and the project "e-Infrastruktura CZ" (e-INFRA LM2018140) provided within the program Projects of Large Research, Development and Innovations Infrastructures. Figures were made using VESTA [36] and gnuplot.

[1] T. Choi, S. Lee, Y. J. Choi, V. Kiryukhin, and S.-W. Cheong, "Switchable ferroelectric diode and photovoltaic effect in bifeo$_3$," Science **324** (2009).

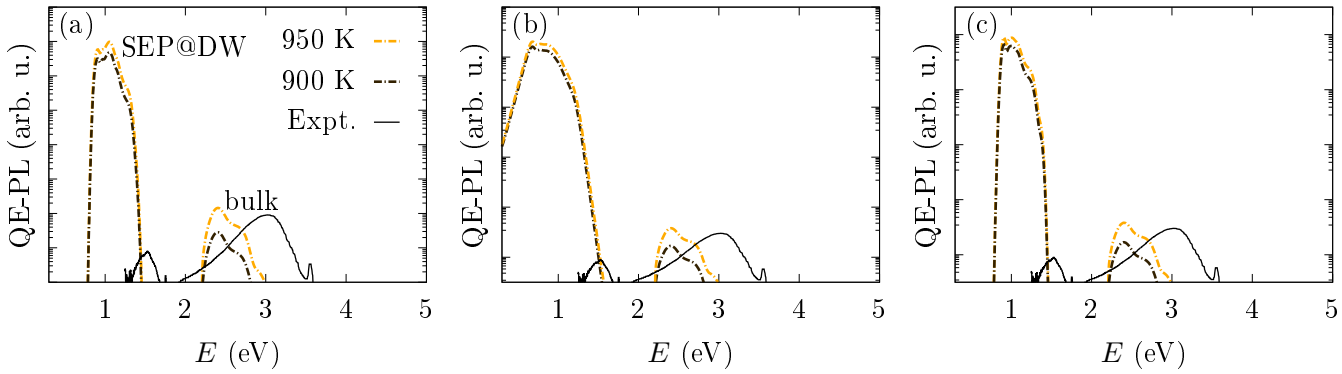

FIG. 9. (Color online) Qualitative estimate of the macroscopically averaged photoluminescence ("QE-PL") spectra of $BiFeO_3$ bulk and domain walls with small electron polarons ("SEP@DW") for two temperatures below the Curie temperature. (a) 71° wall; (b) 109° wall; (c) 180° wall. The experimental spectrum [14] was recorded for a single-domain single crystal at room temperature; here we rescaled its amplitude for better visibility. The peak at 1.5 eV was ascribed to oxygen vacancies.

[2] Akash Bhatnagar, Ayan Roy Chaudhuri, Young Heon Kim, Dietrich Hesse, and Marin Alexe, "Role of domain walls in the abnormal photovoltaic effect in $BiFeO_3$," Nature communications **4** (2013).

[3] Wei Ji, Kui Yao, and Yung C. Liang, "Evidence of bulk photovoltaic effect and large tensor coefficient in ferroelectric $BiFeO_3$ thin films," Phys. Rev. B **84**, 094115 (2011).

[4] Jan Seidel, Lane W Martin, Q He, Q Zhan, Y-H Chu, A Rother, ME Hawkridge, P Maksymovych, P Yu, M Gajek, *et al.*, "Conduction at domain walls in oxide multiferroics," Nat. Mater. **8**, 229–234 (2009).

[5] Sabine Körbel and Stefano Sanvito, "Photovoltage from ferroelectric domain walls in $BiFeO_3$," Phys. Rev. B **102**, 081304(R) (2020).

[6] Delphine Lebeugle, Dorothée Colson, A Forget, and Michel Viret, "Very large spontaneous electric polarization in $BiFeO_3$ single crystals at room temperature and its evolution under cycling fields," Appl. Phys. Lett. **91**, 022907 (2007).

[7] G A Smolenskii, **25**, 475–493 (1982).

[8] S. R. Basu, L. W. Martin, Y. H. Chu, M. Gajek, R. Ramesh, R. C. Rai, X. Xu, , and J. L. Musfeldt, "Photoconductivity in $BiFeO_3$ thin films," Appl. Phys. Lett. **92**, 091905 (2008).

[9] A. J. Hauser, J. Zhang, L. Mier, R. A. Ricciardo, P. M. Woodward, T. L. Gustafson, L. J. Brillson, and F. Y. Yang, "Characterization of electronic structure and defect states of thin epitaxial $BiFeO_3$ films by UV-visible absorption and cathodoluminescence spectroscopies," Appl. Phys. Lett. **92**, 222901 (2008).

[10] JF Ihlefeld, NJ Podraza, ZK Liu, RC Rai, X Xu, T Heeg, YB Chen, J Li, RW Collins, JL Musfeldt, *et al.*, "Optical band gap of $BiFeO_3$ grown by molecular-beam epitaxy," Appl. Phys. Lett. **92**, 142908 (2008).

[11] Amit Kumar, Ram C Rai, Nikolas J Podraza, Sava Denev, Mariola Ramirez, Ying-Hao Chu, Lane W Martin, Jon Ihlefeld, T Heeg, J Schubert, *et al.*, "Linear and nonlinear optical properties of $BiFeO_3$," Appl. Phys. Lett. **92**, 121915 (2008).

[12] V Železný, D Chvostová, L Pajasová, I Vrejoiu, and M Alexe, "Optical properties of epitaxial $BiFeO_3$ thin films," Applied Physics A **100**, 1217–1220 (2010).

[13] Daniel Sando, Cécile Carrétéro, Mathieu N Grisolia, Agnès Barthélémy, Valanoor Nagarajan, and Manuel Bibes, "Revisiting the Optical Band Gap in Epitaxial $BiFeO_3$ Thin Films," Advanced Optical Materials **6**, 1700836 (2018).

[14] Reda Moubah, Guy Schmerber, Olivier Rousseau, Dorothée Colson, and Michel Viret, "Photoluminescence investigation of defects and optical band gap in multiferroic BiFeO3 single crystals," Applied Physics Express **5**, 035802 (2012).

[15] V.M. Fridkin, "Bulk photovoltaic effect in noncentrosymmetric crystals," Crystallogr. Rep. **46**, 654–658 (2001).

[16] S. Y. Yang, J. Seidel, S. J. Byrnes, P. Shafer, C.-H. Yang, M. D. Rossell, Y.-H. Chu P. Yu, J. F. Scott, J. W. Ager III, L. W. Martin, and R. Ramesh, "Above-bandgap voltages from ferroelectric photovoltaic devices," Nat. Nanotechnol. **5**, 143–147 (2010).

[17] Jan Seidel, Deyi Fu, Seung-Yeul Yang, Esther Alarcón-Lladó, Junqiao Wu, Ramamoorthy Ramesh, and Joel W Ager III, "Efficient photovoltaic current generation at ferroelectric domain walls," Phys. Rev. Lett. **107**, 126805 (2011).

[18] Ryotaro Inoue, Shotaro Ishikawa, Ryota Imura, Yuuki Kitanaka, Takeshi Oguchi, Yuji Noguchi, and Masaru Miyayama, "Giant photovoltaic effect of ferroelectric domain walls in perovskite single crystals," Scientific Reports **5**, 14741 (2015).

[19] Oswaldo Diéguez, Pablo Aguado-Puente, Javier Junquera, and Jorge Íñiguez, "Domain walls in a perovskite oxide with two primary structural order parameters: First-principles study of $BiFeO_3$," Phys. Rev. B **87**, 024102 (2013).

[20] Wei Ren, Yurong Yang, Oswaldo Diéguez, Jorge Íñiguez, Narayani Choudhury, and L. Bellaiche, "Ferroelectric Domains in Multiferroic $BiFeO_3$ Films under Epitaxial Strains," Phys. Rev. Lett. **110**, 187601 (2013).

[21] Yi Wang, Chris Nelson, Alexander Melville, Benjamin Winchester, Shunli Shang, Zi-Kui Liu, Darrell G Schlom, Xiaoqing Pan, and Long-Qing Chen, "$BiFeO_3$ domain wall energies and structures: a combined experimental and density functional theory+U study," Phys. Rev. Lett. **110**, 267601 (2013).

[22] Yun-Wen Chen, Jer-Lai Kuo, and Khian-Hooi Chew, "Polar ordering and structural distortion in electronic domain-wall properties of $BiFeO_3$," J. Appl. Phys. **122**, 075103 (2017).

[23] Tadej Rojac, Andreja Bencan, Goran Drazic, Naonori Sakamoto, Hana Ursic, Bostjan Jancar, Gasper Tavcar, Maja Makarovic, Julian Walker, Barbara Malic, *et al.*, "Domain-wall conduction in ferroelectric $BiFeO_3$ controlled by accumulation of charged defects," Nat. Mater. **16**, 322 (2017).

[24] Sabine Körbel, Jirka Hlinka, and Stefano Sanvito, "Electron trapping by neutral pristine ferroelectric domain walls in $BiFeO_3$," Phys. Rev. B **98**, 100104(R) (2018).

[25] Grégory Geneste, Charles Paillard, and Brahim Dkhil, "Polarons, vacancies, vacancy associations, and defect states in multiferroic bifeo$_3$," Phys. Rev. B **99**, 024104 (2019).

[26] Jan Fousek and Václav Janovec, "The orientation of domain walls in twinned ferroelectric crystals," J. Appl. Phys. **40**, 135–142 (1969).

[27] Georg Kresse and Jürgen Furthmüller, "Efficiency of ab-initio total energy calculations for metals and semiconductors using a plane-wave basis set," Comput. Mater. Sci. **6**, 15–50 (1996).

[28] S. L. Dudarev, G. A. Botton, S. Y. Savrasov, C. J. Humphreys, and A. P. Sutton, "Electron-energy-loss spectra and the structural stability of nickel oxide: An LSDA+U study," Phys. Rev. B **57**, 1505–1509 (1998).

[29] Anubhav Jain, Shyue Ping Ong, Geoffroy Hautier, Wei Chen, William Davidson Richards, Stephen Dacek, Shreyas Cholia, Dan Gunter, David Skinner, Gerbrand Ceder, and Kristin A. Persson, "The Materials Project: A materials genome approach to accelerating materials innovation," APL Materials **1**, 011002 (2013), https://doi.org/10.1063/1.4812323.

[30] M Gajdoš, K Hummer, G Kresse, J Furthmüller, and F Bechstedt, "Linear optical properties in the projector-augmented wave methodology," Phys. Rev. B **73**, 045112 (2006).

[31] John David Jackson, *Classical Electrodynamics* (John Wiley & Sons, 1999).

[32] Engin Torun, Henrique PC Miranda, Alejandro Molina-Sánchez, and Ludger Wirtz, "Interlayer and intralayer excitons in MoS_2/WS_2 and $MoSe_2$/WSe_2 heterobilayers," Phys. Rev. B **97**, 245427 (2018).

[33] A F Lima, "Optical properties, energy band gap and the charge carriers' effective masses of the *R*3*c* $BiFeO_3$ magnetoelectric compound," Journal of Physics and Chemistry of Solids **144**, 109484 (2020).

[34] Andjela Radmilovic, Tyler J Smart, Yuan Ping, and Kyoung-Shin Choi, "Combined Experimental and Theoretical Investigations of n-Type BiFeO3 for Use as a Photoanode in a Photoelectrochemical Cell," Chem. Mater. **32**, 3262–3270 (2020).

[35] K Rahmanizadeh, D Wortmann, G Bihlmayer, and S Blügel, "Charge and orbital order at head-to-head domain walls in $PbTiO_3$," Phys. Rev. B **90**, 115104 (2014), https://doi.org/10.1103/PhysRevB.90.115104.

[36] Koichi Momma and Fujio Izumi, "*VESTA3* for three-dimensional visualization of crystal, volumetric and morphology data," J. Appl. Crystallogr. **44**, 1272–1276 (2011).